

# Dislocation Model for Aseismic Crustal Deformation at Hollister, California

MITSUHIRO MATSU'URA

*Geophysical Institute, Faculty of Science, University of Tokyo, Japan*

DAVID D. JACKSON AND ABE CHENG

*Department of Earth and Space Sciences, University of California, Los Angeles*

Geodetic observations at many active plate margins reveal relatively steady aseismic motion during the time between major earthquakes. We model the aseismic motion by the relative motion between several blocks that suffer frictional resistance in the upper crust. Frictional drag is represented by uniform dislocation on a fault surface. We assume that friction occurs only on the upper "brittle zone" of each block boundary and that frictionless sliding occurs below this zone. Using a Bayesian inversion procedure, we invert geodetic data to determine the parameters of the block and dislocation model. Parameters to be estimated include the two horizontal components of velocity for each block and the dislocation rate, dip angle, slip angle, and width of each rectangular fault patch. For Hollister we assume five blocks and nine rectangular fault patches. Rates of length change on 92 lines observed by trilateration make up the data. Triangulation, leveling, very long baseline interferometry, satellite ranging, and global positioning system data can also be easily included in our model. Our inversion procedure uses prior estimates of all block and fault parameters based on geological and seismological data. The block parameters are estimated from geological observations of fault displacement rates, while the widths of the fault patches are estimated from earthquake hypocentral depths. We choose prior estimates of the dislocation rate to match observed creep rates. The estimated block motion is well resolved by the geodetic data and agrees well with the geological estimates. This suggests that the block motion is steady on time scales from 10 years to 1 m.y. The net motion across the San Andreas-Calaveras fault system is  $38 \pm 3$  mm/yr oriented S38°E. Thus some additional displacement, possibly offshore, is needed to match the rate of 56 mm/yr predicted by plate tectonic models. The depth of the transition from frictional to free sliding varies considerably, from 0.4 km on the southern Calaveras to 11 km on the central San Andreas fault. Two segments of the San Andreas, north of 36°50' and south of 36°40', have the greatest potential for moderate to large earthquakes.

## 1. INTRODUCTION

Since 1971, the U.S. Geological Survey (USGS) has frequently repeated line length measurements on trilateration networks which span the San Andreas fault system in California [Savage *et al.*, 1979, 1981]. The trilateration data contain important information about the accumulation and release of tectonic stress on the plate boundary.

In most cases, trilateration data have been analyzed under the assumption of uniform strain in space or uniform slip on one or two fault planes. However, these assumptions seem too simple to interpret actual crustal deformation in a fault zone. Moreover, for precise analysis, a systematic, robust method is necessary, since the data are contaminated by noise.

In this study we first introduce a dislocation model for aseismic crustal deformation near the plate boundary. Second, we develop a method for inverting trilateration data on the basis of a new algorithm for nonlinear inversion. Finally, the method is applied to the trilateration data for the USGS Hollister network.

Savage *et al.* [1979] and Thatcher [1979] have both analyzed geodetic data for the Hollister area in terms of simple dislocation models. By using few model parameters they have ignored spatial variations in stress accumulation rate that we find to be significant. We compare our specific results with their results in section 6.

We are able to include more model parameters, and thus obtain a more realistic model, because we use a new nonlinear

inversion procedure employing prior estimates of all parameters. This Bayesian inversion procedure, summarized briefly below, is described in complete detail by Jackson and Matsu'ura [1985].

## 2. A DISLOCATION MODEL FOR ASEISMIC DEFORMATION

Consider the stress accumulation and release caused by the relative motions of several elastic blocks with friction between them. We assume that each block boundary may be divided into an upper "brittle" zone and a lower "ductile" zone. The simple case of two blocks separated by a vertical boundary is illustrated in Figure 1. We suppose that the shallower part of the boundary is locked in an interseismic stage, while the deeper part is completely free. The blocks are subject to a uniform relative motion parallel to the boundary. Then, as a result of the relative motion, tectonic stress accumulates in the shallower locked part. When the tectonic stress on the boundary reaches an ultimate value, rupture occurs so as to release the accumulated stress. Tectonic stress then begins to accumulate again for some future event.

In the interseismic stage, crustal deformation near the block boundary may be regarded as the sum of a rigid block motion and the effect of the locked part. As is seen from Figure 1, the effect of the locked part is equivalent to that of a negative dislocation on the boundary. Here, the negative sign is taken so that the dislocation corresponds to the slip deficit, presumably to be paid back in some forthcoming earthquake. Then we may interpret the aseismic crustal deformation as a result of the rigid block motion and the negative dislocation on the boundary.

Copyright 1986 by the American Geophysical Union.

Paper number 6B5945.  
0148-0227/86/006B-5945\$05.00

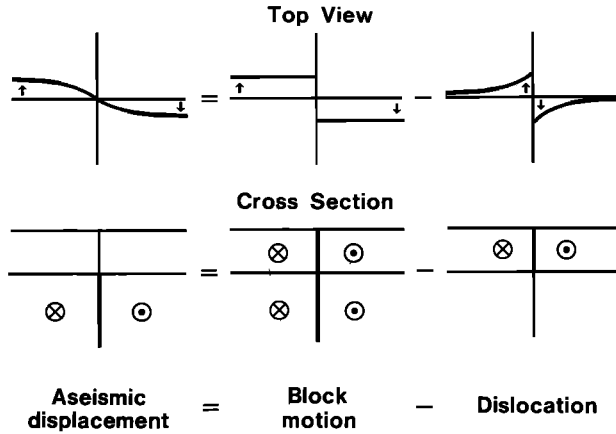


Fig. 1. Model for aseismic crustal deformation at a block boundary. The aseismic displacement (left) is the difference between pure block motion (center) and the displacement due to the slip deficit, represented by a dislocation in the upper locked part (right). This diagram shows a special case: the dislocation rate equals the relative block motion, so there is no surface creep.

More generally, the upper brittle zone may be divided into several rectangular patches, each having its own length, width, dip, and strike. We assume the slip to be spatially uniform within each rectangular patch and within the lower zone bounding each pair of contiguous blocks. We then infer the average slip rate on each of the patches, and on the lower boundaries, from the average rates of line length change between pairs of monuments on the earth's surface.

Our conceptual model is similar to the dislocation loop model of *Savage et al.* [1979] for the upper brittle zone. For the lower, freely slipping zone, they assumed a patch extending to 1000 km depth, effectively infinite compared to the horizontal extent of the geodetic network. They assumed, as we do, that the slip is uniform within each patch. We define the slip on the lower part of each boundary to be the relative displacement of the two blocks in contact there. Because friction near the earth's surface generally impedes block motion, we allow for a slip deficit on the upper fault patches. We model this deficit by a uniform dislocation on each patch. The net slip is then the difference between relative block motion and the dislocation motion on the patch. If the near-surface patches were locked (no slip), then the dislocation motion would precisely equal the block motion, and the two would cancel. We chose this representation for the following reasons:

1. It is mathematically more convenient than the dislocation loop representation.
2. It predicts that monuments far from the block boundaries would move with their respective plates. We believe this model is physically more realistic than the dislocation loop model, which predicts no displacement for such monuments.
3. The dislocation motion on the fault patches has a useful physical interpretation: it is the slip deficit on the fault patches, and the rate of stress accumulation is proportional to it.

Our block and dislocation model will be mathematically equivalent to the dislocation loop model of *Savage et al.* [1979] when the block boundaries are vertical, when the bottom depth of their lower loop is infinite, when our relative block motion is parallel to the boundary, and when our dislocation motion is purely horizontal. These conditions are nearly satisfied in the case of Hollister. Both models predict discontinuous slip rates, infinite strains, and "sources and sinks" of matter along the edges of the patches. These con-

ditions could be viewed as unphysical if the models were interpreted literally. However, we do not pretend that the slip is actually uniform within each patch; rather, we presume that the slip varies continuously over the fault and the "uniform" slip on each patch is just the average value on that part of the fault surface.

Our block and dislocation model does have some features absent from the dislocation loop model. The most important one is that our model allows dip-slip motion on the block boundaries and a variable dip angle to be determined by the data. In fact, there must be some dip-slip motion if there are more than three independent blocks, unless all block boundaries are parallel to one another. Our model correctly accounts for the resulting block motion far from the boundary, but neither our model nor the dislocation loop model correctly describes the resulting elastic effects near the boundary.

### 2.1. Line Length Change

We take a Cartesian coordinate system  $(X, Y)$  as a frame of reference. Let the coordinates of the  $i$ th trilateration station  $P^i$  be  $(X^i, Y^i)$  at  $t = t_0$  and  $(X^i + W_X^i, Y^i + W_Y^i)$  at  $t = t_0 + \Delta t$ . Here,  $\mathbf{W}^i = (W_X^i, W_Y^i)$  indicates the total displacement vector of  $P^i$  in the time interval from  $t_0$  to  $t_0 + \Delta t$ . Then, denoting the line length between  $P^i$  and  $P^j$  at  $t = t_0$  by  $l_0^{ij}$ , the change of the line length during the interval from  $t_0$  to  $t_0 + \Delta t$  is given by

$$\Delta l^{ij} = \sin \theta^{ij}(W_X^j - W_X^i) + \cos \theta^{ij}(W_Y^j - W_Y^i) \quad (1)$$

with

$$\sin \theta^{ij} = (Y^j - Y^i)/l_0^{ij} \quad \cos \theta^{ij} = (X^j - X^i)/l_0^{ij} \quad (2)$$

under the condition,

$$|\mathbf{W}^i - \mathbf{W}^j| \ll l_0^{ij} \quad (3)$$

In actual cases the line length  $l_0^{ij}$  is of the order of several kilometers, while the magnitude of displacement vectors  $|\mathbf{W}^i|$  and  $|\mathbf{W}^j|$  are much less than 1 m, so the above condition is always satisfied.

### 2.2. Aseismic Crustal Deformation

In our model the aseismic crustal deformation is regarded as a result of the rigid block motion and the negative dislocation on the locked parts of block boundaries. Then the total displacement vector  $\mathbf{W}^i = (W_X^i, W_Y^i)$  at the  $i$ th station can be written as

$$\mathbf{W}^i = \mathbf{V}^i - \mathbf{U}^i \quad (4)$$

where  $\mathbf{V}^i = (V_X^i, V_Y^i)$  is the displacement vector of a block in which the  $i$ th station is located and  $\mathbf{U}^i = (U_X^i, U_Y^i)$  is the displacement vector at the  $i$ th station due to the dislocation on the locked parts.

Now we consider the simplest case in which a system of interacting plates is modeled by two blocks and one fault plane (locked part). In such a case the displacement vector due to the block motion, which is assumed to be uniform in each block, is

$$\mathbf{V}^i = \mathbf{V}(X = X^i, Y = Y^i; V_X(1), V_Y(1), V_X(2), V_Y(2)) \quad (5)$$

with

$$\begin{aligned} \mathbf{V}(X, Y) &= \mathbf{V}(1) & \text{if } X \text{ lies within block 1} \\ \mathbf{V}(X, Y) &= \mathbf{V}(2) & \text{if } X \text{ lies within block 2} \end{aligned} \quad (6)$$

where  $\mathbf{V}(1) = [V_X(1), V_Y(1)]$  and  $\mathbf{V}(2) = [V_X(2), V_Y(2)]$  are con-

stant vectors. On the other hand, the displacement vector due to uniform slip on a rectangular fault plane is uniquely determined by a set of nine independent parameters as shown in Figure 2; that is,

$$U' = U(X = X', Y = Y'; D, \delta, \lambda, W, d, a_x, a_y, b_x, b_y) \quad (7)$$

Here,  $D$  is the magnitude of dislocation,  $\delta$  is a dip angle;  $\lambda$  is a slip angle,  $W$  is a fault width,  $d$  is a depth to the upper fault edge,  $(a_x, a_y)$  are the coordinates of the upper left fault corner, and  $(b_x, b_y)$  are the coordinates of the upper right fault corner.

It is reasonable to assume that the locked part extends to the earth's surface. Moreover, in most cases, we know the fault trace and its extent from geological observations. Then, in place of (7), we have

$$U(X, Y) = U(X, Y; D, \delta, \lambda, W) \quad (8)$$

In a similar way, we can treat more complicated cases. For example, when the system consists of  $p$  blocks and  $q$  fault patches, (6) is replaced by

$$V(X, Y) = V(k) \quad \text{if } X \text{ lies within block } k \quad (9)$$

$$(k = 1, \dots, p)$$

and (8) by

$$U(X, Y) = \sum_{k=1}^q U^{(k)}(X, Y; D^{(k)}, \delta^{(k)}, \lambda^{(k)}, W^{(k)}) \quad (10)$$

### 2.3. Forward Model and Partial Derivatives

From (1) and (4) we may express the line length change  $\Delta l^{ij}$  as a function of model parameters:

$$\Delta l^{ij} = f^{ij}(V_x(1), V_y(1), V_x(2), V_y(2), D, \delta, \lambda, W) \quad (11)$$

The functional form of  $f^{ij}$  is given by

$$f^{ij} = \sin \theta^{ij} [V_x]_i^j + \cos \theta^{ij} [V_y]_i^j - \sin \theta^{ij} [U_x]_i^j - \cos \theta^{ij} [U_y]_i^j \quad (12)$$

Here, it is noted that  $V_x$  is a function of  $V_x(1)$  and  $V_x(2)$ ,  $V_y$  is a function of  $V_y(1)$  and  $V_y(2)$ , and  $U_x$  and  $U_y$  are functions of  $D$ ,  $\delta$ ,  $\lambda$ , and  $W$ . The symbol  $[ ]_i^j$  indicates that

$$[F(\mathbf{X})]_i^j \equiv F(\mathbf{X}^j) - F(\mathbf{X}^i) \quad (13)$$

Partial derivatives of  $f^{ij}$  with respect to the model parameters, which are needed to construct a coefficient matrix in the next section, are calculated as follows:

For  $V_x(1)$ ,  $V_y(1)$ ,  $V_x(2)$ , and  $V_y(2)$ ,

$$\frac{\partial f^{ij}}{\partial V_x(k)} = \sin \theta^{ij} \left[ \frac{\partial V_x}{\partial V_x(k)} \right]_i^j \quad k = 1, 2$$

$$\frac{\partial f^{ij}}{\partial V_y(k)} = \cos \theta^{ij} \left[ \frac{\partial V_y}{\partial V_y(k)} \right]_i^j \quad k = 1, 2 \quad (14)$$

with

$$\frac{\partial V_x}{\partial V_x(k)} = \frac{\partial V_y}{\partial V_y(k)} = 1 \quad \text{if } \mathbf{X} \text{ lies within block } k$$

$$\frac{\partial V_x}{\partial V_x(k)} = \frac{\partial V_y}{\partial V_y(k)} = 0 \quad \text{otherwise} \quad (15)$$

For  $D$ ,  $\delta$ ,  $\lambda$ , and  $W$ , denoting any of these parameters by  $\alpha$ ,

$$\frac{\partial f^{ij}}{\partial \alpha} = -\sin \theta^{ij} \left[ \frac{\partial U_x}{\partial \alpha} \right]_i^j - \cos \theta^{ij} \left[ \frac{\partial U_y}{\partial \alpha} \right]_i^j \quad (16)$$

We take a Cartesian coordinate system  $(x, y, z)$  fixed to the

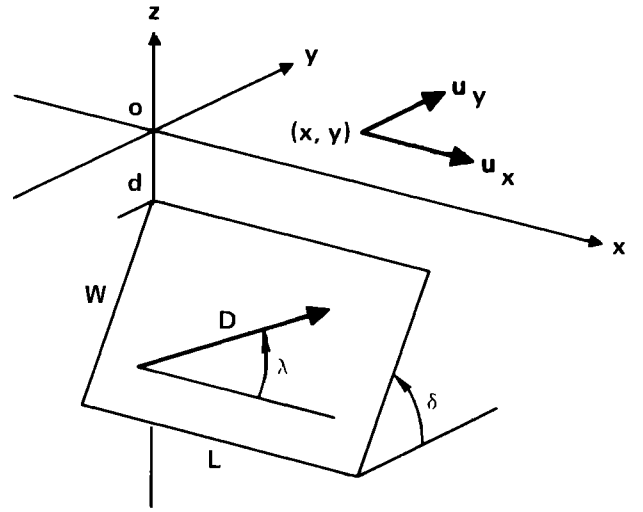


Fig. 2. Fault geometry and notation.  $D$  is the dislocation magnitude,  $\delta$  is the dip angle,  $\lambda$  is the slip angle,  $W$  is the width,  $d$  is the depth to the upper fault edge, and  $u_x$  and  $u_y$  are the  $x$  and  $y$  component of the surface displacement in the coordinate system fixed to the fault.

fault as shown in Figure 2. The displacement components  $u_x$  and  $u_y$  in this coordinate system are related to the displacement components  $U_x$  and  $U_y$  in the reference coordinate system  $(X, Y)$  as

$$U_x(X, Y) = \sin \phi u_x(x, y) - \cos \phi u_y(x, y)$$

$$U_y(X, Y) = \cos \phi u_x(x, y) + \sin \phi u_y(x, y) \quad (17)$$

with

$$x = \sin \phi (X - a_x) + \cos \phi (Y - a_y)$$

$$y = -\cos \phi (X - a_x) + \sin \phi (Y - a_y) \quad (18)$$

where  $\phi$  is the angle of fault strike measured clockwise from the  $Y$  axis. Then, for the partial derivatives of displacement with respect to the fault parameters we have

$$\frac{\partial U_x}{\partial \alpha} = \sin \phi \frac{\partial u_x}{\partial \alpha} - \cos \phi \frac{\partial u_y}{\partial \alpha}$$

$$\frac{\partial U_y}{\partial \alpha} = \cos \phi \frac{\partial u_x}{\partial \alpha} + \sin \phi \frac{\partial u_y}{\partial \alpha} \quad (19)$$

Matsu'ura [1977] gives analytical expressions for the surface displacement field, and its partial derivatives with respect to fault parameters, of a rectangular fault. Okada [1985] gives an excellent and comprehensive review of computing methods for surface deformations due to faulting.

### 2.4. Length Change Rates

If the process of strain accumulation is considered to be uniform in time, instead of (11), we have

$$l^{ij} \equiv \frac{\Delta l^{ij}}{\Delta t} = f^{ij}(\dot{V}_x(1), \dot{V}_y(1), \dot{V}_x(2), \dot{V}_y(2), \dot{D}, \delta, \lambda, W) \quad (20)$$

Here,  $l^{ij}$  is the rate of line length change;  $\dot{V}(1)$  and  $\dot{V}(2)$  are the velocity vectors of the block 1 and block 2, respectively; and  $\dot{D}$  is the rate of dislocation on the fault.

In reality, the strain rate is not constant in time. We assume that steady strain accumulation dominates but that episodic slip motion, especially on the upper parts of block boundaries, will punctuate the strain accumulation. The average rate of

line length change over a long enough time interval will reflect the secular block velocities and fault slip rates, while residual length variations give a measure of the episodic effects (mixed, of course, with experimental errors). Thus we shall use (20), with average rates of line length change as the basic data, and interpret the arguments of the right-hand side as averages over the relevant time interval. We shall use data sets covering slightly different time intervals to test the hypothesis that the process of strain accumulation is constant in time. Of course, we also want to know whether the average block velocities deduced from just a few years of geodetic observation are at all similar to the geologically observed block velocities, which are averages over many thousands of years.

### 3. NONLINEAR INVERSION PROCEDURE

Our problem is to estimate simultaneously the fault parameters and the block velocities from the trilateration data. In most cases, the problem is ill-conditioned because the stations are sparse and the data are noisy. Line length rates are nearly linear functions of the block velocities and dislocation rates, but they are nonlinear functions of fault width and the dip and slip angles.

Jackson [1979] demonstrated that an ill-conditioned linear inverse problem can be reduced to a well-conditioned problem by incorporating sufficient prior data. Then the problem may be solved by using the classical least squares procedure. The use of prior information about model parameters is essential, since any solution depends inevitably on the initial guess of model parameters when the problem is underdetermined [Matsu'ura and Hirata, 1982]. Tarantola and Valette [1982] have extended Jackson's approach to nonlinear cases by defining the least squares problem before linearization.

Recently, Jackson and Matsu'ura [1985] developed a new algorithm of nonlinear inversion from a Bayesian point of view. In this section we describe it briefly.

#### 3.1. Fundamental Equations

Let us consider a set of observational equations in vector form:

$$\mathbf{y}^0 = \mathbf{f}(\mathbf{x}) + \mathbf{e} \quad (21)$$

where  $\mathbf{y}^0$  is an  $n$  vector of observed data,  $\mathbf{x}$  is an  $m$  vector of model parameters,  $\mathbf{f}$  is an  $n$  vector of nonlinear functions of  $\mathbf{x}$ , and  $\mathbf{e}$  is an  $n$  vector of random errors. The random errors  $\mathbf{e}$  are supposed to be Gaussian with zero mean and a covariance matrix  $\mathbf{E}$ .

In geophysical problems we have some information about model parameters before the collection of observed data. We express the prior information in the form of

$$\mathbf{x}^0 = \mathbf{x} + \mathbf{d} \quad (22)$$

where  $\mathbf{x}^0$  is an  $m$  vector of prior estimates of  $\mathbf{x}$ , and  $\mathbf{d}$  is an  $m$  vector of random errors. The random errors  $\mathbf{d}$  are also supposed to be Gaussian with zero mean and a covariance matrix  $\mathbf{D}$ . The prior estimates of model parameters will generally be correlated, so that the covariance matrix  $\mathbf{D}$  will have off-diagonal elements. This case arises especially when the prior estimates result from inversion of a different data set, independent of the observations used here. Sometimes the prior information may arise from physical constraints on the parameters, and the uncertainty in this information may be represented by a diagonal covariance matrix.

According to Bayes' theorem, the conditional probability

density of  $\mathbf{x}$  given  $\mathbf{y}^0$  is

$$p(\mathbf{x}|\mathbf{y}^0) = c \cdot \exp \left[ -\frac{1}{2} s(\mathbf{x}) \right] \quad (23)$$

with

$$s(\mathbf{x}) = \mathbf{e}'\mathbf{E}^{-1}\mathbf{e} + \mathbf{d}'\mathbf{D}^{-1}\mathbf{d} \quad (24)$$

where

$$\mathbf{e} = \mathbf{y}^0 - \mathbf{f}(\mathbf{x}) \quad (25)$$

and

$$\mathbf{d} = \mathbf{x}^0 - \mathbf{x} \quad (26)$$

The superscript "t" indicates the transpose of the corresponding matrix or column vector. The first term of (24) represents the weighted sum of squared residuals for the observations and the second term represents the same quantity for the prior data. The inverse covariance matrices  $\mathbf{E}^{-1}$  and  $\mathbf{D}^{-1}$  weight the observations and prior data, respectively, so that uncertain data get little weight.

The maximum likelihood estimate of  $\mathbf{x}$  is given by the vector  $\hat{\mathbf{x}}$  which maximizes the conditional probability density  $p(\mathbf{x}|\mathbf{y}^0)$ , and the maximum of  $p(\mathbf{x}|\mathbf{y}^0)$  is realized by minimizing the quadratic form  $s(\mathbf{x})$ . For any solution which minimizes  $s(\mathbf{x})$ , the variation of  $s(\mathbf{x})$  with respect to  $\mathbf{x}$  must vanish. Thus we obtain fundamental equations to be solved for  $\hat{\mathbf{x}}$ :

$$\mathbf{A}'\mathbf{E}^{-1}\mathbf{e} + \mathbf{D}^{-1}\mathbf{d} = \mathbf{0} \quad (27)$$

where  $\mathbf{A}$  represents an  $n \times m$  matrix defined by

$$\mathbf{A} = \text{grad } \mathbf{f}(\mathbf{x})|_{\mathbf{x}=\hat{\mathbf{x}}} \quad (28)$$

whose elements are  $A_{ij} = (\partial f_i / \partial x_j)|_{\mathbf{x}=\hat{\mathbf{x}}}$

#### 3.2. Solution to the Fundamental Equations

The nonlinear equations in (27) may be solved by using an iterative procedure. For an arbitrary fixed point  $\mathbf{x}_k$  a simple algorithm of iterative search for the solution is given by

$$\mathbf{x}_{k+1} = \mathbf{x}_k + \alpha_k (\mathbf{A}_k' \mathbf{E}^{-1} \mathbf{A}_k + \mathbf{D}^{-1})^{-1} \mathbf{r}_k \quad 0 < \alpha_k \leq 1 \quad (29)$$

with

$$\mathbf{r}_k = \mathbf{A}_k' \mathbf{E}^{-1} [\mathbf{y}^0 - \mathbf{f}(\mathbf{x}_k)] + \mathbf{D}^{-1} (\mathbf{x}^0 - \mathbf{x}_k) \quad (30)$$

and

$$\mathbf{A}_k = \text{grad } \mathbf{f}(\mathbf{x})|_{\mathbf{x}=\mathbf{x}_k} \quad (31)$$

Here,  $\alpha_k$  is a factor to adjust the length of the correction vector. For mildly nonlinear problems the factor  $\alpha_k$  is safely set to 1. If we have no prior information about the parameters, then  $\mathbf{D}^{-1} = \mathbf{O}$ , and (29) reduces to the standard Gauss-Newton method for nonlinear least squares problems. However, in most geophysical problems we do have useful prior information, even if it may not be adequate for our needs.

From (27) it is clear that  $\mathbf{r}_k$  tends to a null vector as  $\mathbf{x}_k$  approaches the solution  $\hat{\mathbf{x}}$  if  $\mathbf{f}(\mathbf{x})$  are continuous functions of  $\mathbf{x}$ . We can thus use the norm of  $\mathbf{r}_k$  to judge the convergence of the iterative process. In practice, denoting a certain threshold by  $\gamma$ , the solution  $\hat{\mathbf{x}}$  is defined as

$$\hat{\mathbf{x}} = \mathbf{x}_k \quad \text{if } \|\mathbf{r}_k\|^2 < \gamma \quad (32)$$

#### 3.3. Evaluation of Estimation Errors

For the final estimates  $\hat{\mathbf{x}}$  we can evaluate the covariance of estimation errors directly from the fundamental equations (27) under the assumption of linearity for  $\mathbf{f}(\mathbf{x})$  at  $\mathbf{x} = \hat{\mathbf{x}}$ . The asymptotic covariance matrix of the estimation error is given

by

$$\mathbf{C} = (\mathbf{A}'\mathbf{E}^{-1}\mathbf{A} + \mathbf{D}^{-1})^{-1} \quad (33)$$

where the matrix  $\mathbf{A}$  is the same as that in (28). If the functions  $\mathbf{f}(\mathbf{x})$  are nearly linear within some reasonable confidence region about  $\hat{\mathbf{x}}$ , then (33) will give a good approximation to a true covariance matrix.

*Jackson and Matsu'ura* [1985] show that the posterior variance of any parameter obtained from  $\mathbf{C}$  must be less than or equal to the prior variance obtained from  $\mathbf{D}$ . Assuming that  $\mathbf{E}$  and  $\mathbf{D}$  truly represent the errors in the observed data and prior estimates, then the expected value of the quantity  $s(\mathbf{x})$  in (24) is equal to  $n$ , the number of observed data (there are  $n + m$  total data, and  $m$  parameters, so there are  $n$  degrees of freedom in the residuals). Often the realized value of  $s$  differs significantly from its expected value, implying that the data uncertainties have been either underestimated or overestimated. The assumed covariance matrices  $\mathbf{E}$  and  $\mathbf{D}$  are only estimates of the true covariances, so they are themselves subject to error.  $\mathbf{E}$  should describe all of the random effects on measured line lengths that are not explicitly modeled: such things as random errors in line length measurements, errors in the refraction corrections, setup errors, small blunders, monument instability, soil motion, displacements on neglected faults, etc. As a first approximation, we estimate the variance of length rates for each line from the linearity of measured length with respect to time. To the extent that any of the error sources may be correlated with time, they will escape detection. Similarly,  $\mathbf{D}$  should describe the errors in our prior estimates, including errors in the geological and seismological data, temporal variations in displacement rate, neglect of smaller faults, etc. To allow for errors in the preliminary covariance estimates, we use a modified form of (33):

$$\mathbf{C}' = \sigma^2(\mathbf{A}'\mathbf{E}^{-1}\mathbf{A} + \mathbf{D}^{-1})^{-1} \quad (34)$$

where  $\sigma^2$  is the variance inflation factor,

$$\sigma^2 = s/n \quad (35)$$

With this modification the posterior uncertainty of a given parameter, or linear combination of parameters, may exceed the prior uncertainty by the factor  $\sigma$ , at most.

#### 3.4. Resolution of Parameter Estimates

Under the assumption of linearity for  $\mathbf{f}(\mathbf{x})$  at  $\mathbf{x} = \hat{\mathbf{x}}$  we can also define the asymptotic resolution matrix as

$$\mathbf{R} = \mathbf{I} - \mathbf{C}\mathbf{D}^{-1} \quad (36)$$

$\mathbf{R}$  is the usual resolution matrix [e.g., *Jackson*, 1972] relating the estimate  $\hat{\mathbf{x}}$  to the general solution  $\mathbf{x}$ . *Jackson and Matsu'ura* [1985] show that the diagonal elements of the resolution matrix may be interpreted as the fraction of information provided by the observations about each of the parameters. The complement of the resolution matrix gives the fraction provided by the prior data. Thus, when the diagonal elements of the resolution matrix are near 1.0, the parameter estimates are insensitive to the prior data.

In the special case that  $\mathbf{D}$  is diagonal, then the diagonal elements of the resolution matrix are given by

$$R_{ii} = 1 - C_{ii}/D_{ii} \quad (37)$$

The resolution of any parameter is simply one minus the ratio of its posterior variance to its prior variance. For well-resolved parameters the posterior variance is much smaller than the prior variance, and the resolution is near one. For

poorly resolved parameters the posterior variance almost equals the prior variance, and the resolution is nearly zero.

#### 4. ANALYSIS OF STRAIN ACCUMULATION NEAR HOLLISTER

In the preceding sections we developed an inverse method for analyzing trilateration data. As an example, we apply this method to observed data for the Hollister network which spans the junction of the Calaveras and San Andreas faults in central California. The location map is given in Figure 3.

##### 4.1. Trilateration Data

We used data for the USGS Hollister network, kindly provided by J. Savage and his coworkers at USGS in Menlo Park. The network has been surveyed approximately annually since 1971. Figure 4 shows the locations of the trilateration monuments, the lines used in our analysis, and the surface traces of the larger mapped faults in the region. Our three-letter station codes consist of the first three consonants of the station names used by *Savage et al.* [1979] with the following exceptions: HLR, Hollair; HLS, Hollis; and OAK, Oak.

We analyzed three different versions of the basic data set to test the effect of various assumptions. The three data sets are labeled by the latest year for which data are included and the number of lines used. Data consist of average rates of line length change, estimated by linear regression of the line length on time. Standard deviations of the length change rates are based on the residuals to this linear regression. In our modeling, we weighted each datum by its inverse standard deviation. The data sets are as follows.

Data set 78/69 consists of average length change rates from 1971 through 1978 for 69 lines. These data are identical to those reported and interpreted by *Savage et al.* [1979] except that 16 lines involving stations HLS and PRR have been given zero weight. We gave them zero weight because the true location of the Calaveras fault with respect to these stations is doubtful and the relative locations may strongly affect the results for such a shallow fault. By including the questionable lines with zero weight we provide that the parameter estimates are independent of these data, but theoretical rates and residuals are still computed for these lines. Except for these 16 lines with zero weight, this data set is identical with data set 78/85, described next.

Data set 78/85 consists of average length change rates from 1971 through 1978 for 85 lines. The data set is identical to that reported by *Savage et al.* [1979]. The 16 lines to HLS and PRR are included with no special treatment.

Data set 83/92 consists of average length change rates from 1971 through 1983 for the 85 lines used above and the seven lines to station BLS (Bolsarm2). Baselines from LNT were not observed after 1978, and baselines from BLS were not observed before that year. This change in station coverage could introduce a spurious spatial variation in deformation if there were a temporal change in displacement rate about 1978. However, there is no evidence for any large change in rate, and our error estimates are adequate to cover any likely variations.

##### 4.2. Fault Geometry

We assumed five blocks separated by nine idealized fault segments as shown in Figure 5. The block names were chosen to be mnemonics for east, west, north, central, and "extra." Figure 5 also contains some final results to the discussed below. Figures 4 and 5 share the same scale. Obviously, we had to take some liberties with the mapped fault traces, es-

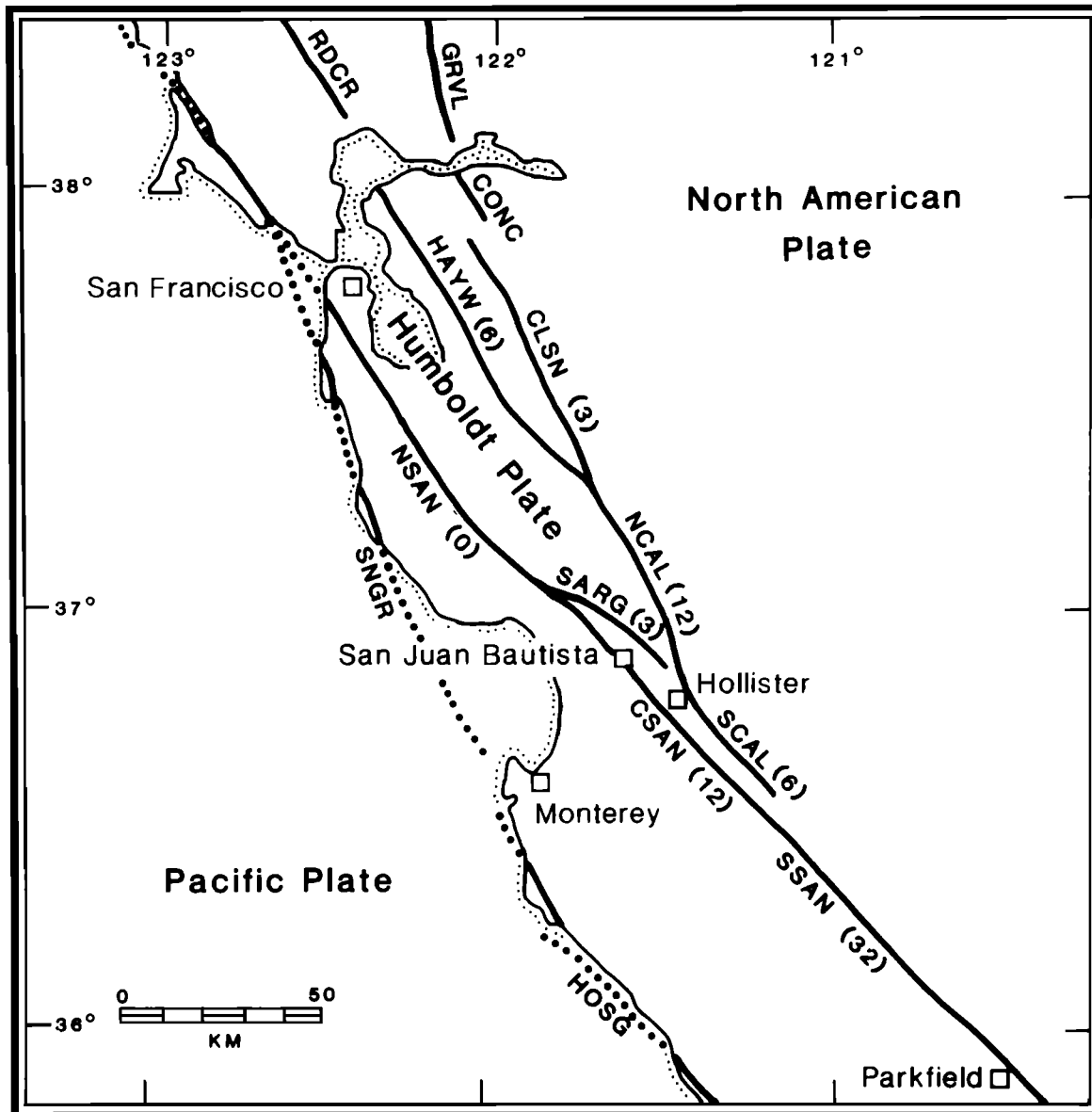


Fig. 3. Location map showing principal active faults in central California, modified from *Ellsworth et al.* [1981]. Average creep rates in millimeters per year appear in parentheses following fault name code. The creep data are from *Herd* [1979], *Burford and Harsh* [1980], and *Ellsworth et al.* [1981]. Fault codes are as follows: NSAN, northern San Andreas; CSAN, central San Andreas; SSAN, southern San Andreas; NCAL, northern Calaveras; SCAL, southern Calaveras; SARG, Sargent; SNGR, San Gregorio; HOSG, Hosgri; GRVL, Green Valley; CONC, Concord; CLSN, Calaveras-Sunol; RDCR, Rodgers Creek; HAYW, Hayward.

pecially with the southern Calaveras and Sargent faults (SCAL and SSAR). Our results will not depend strongly on minor changes in fault location for those faults which are locked to a depth of several kilometers, but changes in fault location could be important for faults with a small locking depth or with substantial creep. It was this concern that led us to make separate calculations for data set 78/69, giving special treatment to stations near SCAL. The boundaries between NSAN, CSAN, and SSAN were chosen at places where the mapped fault trace changes direction. The northern ends of NSAN, NCAL, and NSAR are chosen somewhat arbitrarily, as is the southern end of SSAN. These faults have been assigned arbitrary lengths of 100 km, 100 km, 100 km and 200 km, respectively. The values chosen will have little effect on the results because the ends of these faults are so far away from any of the monuments used in this work.

#### 4.3. Primary Parameters

Parameters in our model include the eastward and northward velocities of the five blocks and four parameters (dislocation rate, dip angle, slip angle, and fault width) for each of nine fault segments. We have 46 parameters to be determined by the data. We effectively fixed the western block as the origin of coordinates by including prior data as described below. This choice is quite arbitrary, as only the relative block velocities have any meaning in this analysis.

#### 4.4. Derived Parameters

We also computed estimates for several derived parameters:

Block slip rate

$$s_b = [\dot{V}(j) - \dot{V}(i)] \cdot t \quad (38)$$

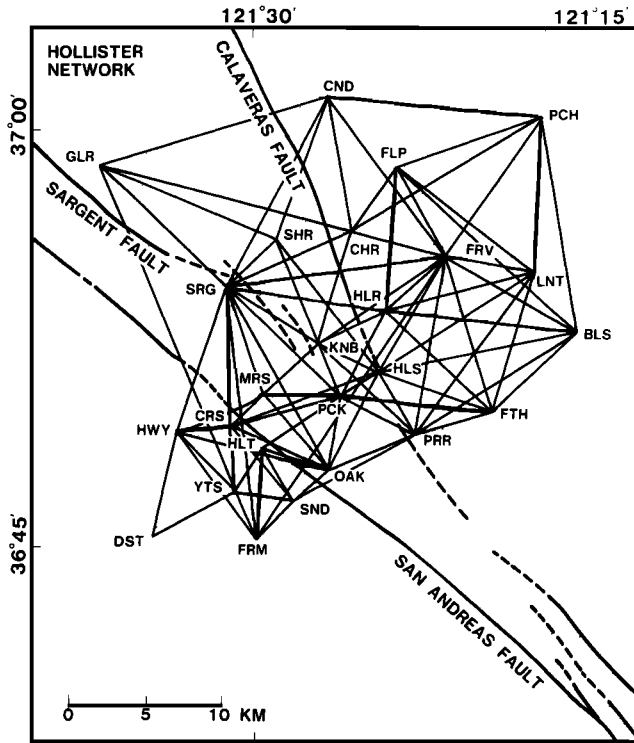


Fig. 4. Hollister trilateration network, modified from Savage et al. [1979]. Mapped faults are shown by thick lines, dashed where the fault trace is uncertain.

Block convergence rate

$$c_b = [\dot{V}(j) - \dot{V}(i)] \cdot \mathbf{n} \quad (39)$$

Fault slip rate

$$s_f = -\dot{D} \cos \lambda \quad (40)$$

Fault convergence rate

$$c_f = \dot{D} \sin \lambda \cos \delta \quad (41)$$

Creep rate

$$r_c = s_b - s_f \quad (42)$$

In these expressions,  $\dot{V}(i)$  and  $\dot{V}(j)$  represent the velocity vectors of the two blocks separated by the fault in question,  $\mathbf{t}$  is a unit vector parallel to the fault trace (reckoned positive for right-lateral slip),  $\mathbf{n}$  is a unit vector normal to the fault trace (reckoned positive for convergence), and dot product represents a scalar product. The block slip rate and block convergence rate are relevant to the lower, freely slipping part of the block boundary. The fault slip rate is the strike-slip component of the dislocation rate; a positive value corresponds to right-lateral slip deficit. The fault convergence rate is the projection of the dip-slip component of the dislocation rate on the earth's surface. A positive value corresponds to a convergence deficit. The creep rate is the net horizontal slip on the shallow part of the block boundary (the fault patch) after correcting the block slip rate for the negative contribution of the fault slip rate. Taking our model literally, one should expect the creep rate to match the observed creep on major faults. We do not take the model quite so literally, since the assumptions of the model are not valid near the fault edges.

The pattern of displacements has implications for stress accumulation, recurrence interval, and maximum seismic displacement on each of the fault segments. Roughly, we expect

that the rate of stress accumulation should be proportional to the dislocation rate  $\dot{D}$  and inversely proportional to the fault width  $W$ . The recurrence interval for the largest earthquakes should be inversely proportional to the rate of stress accumulation, and the seismic displacement in such events should be the cumulative elastic displacement between events (that is, the product of the recurrence interval and the dislocation rate).

As Weertman [1965] pointed out, the stress increment on a long vertical strike-slip fault can in principle be deduced from the resulting surface displacements. However, in practice, radically different stress distributions lead to nearly equal surface displacements. Our block and dislocation model represents rather well the average displacement at depth and near the earth's surface. However, the rate of stress accumulation depends on how sharp the transition is from the brittle zone to the ductile zone, and our model fails to represent this transition. For computational convenience we assume abrupt displacement discontinuities at the edges of each fault segment; these discontinuities cause nasty singularities in the theoretical stress. In nature the transitions from one fault to another, and from each fault to the freely slipping zone below it, must be smooth enough to avoid such singularities.

To relate stress and displacement on the fault surface, we shall adopt results for a slightly more realistic model, knowing that it also may be quite imperfect in some details. Knopoff [1958] showed that a uniform stress drop "S" on an infinitely long, vertical strike-slip surface fault of width "a" leads to the displacement offset of the form

$$u(z) = \frac{2aS}{\mu} [1 - (z/a)^2]^{1/2} \quad 0 \leq z \leq a \quad (43)$$

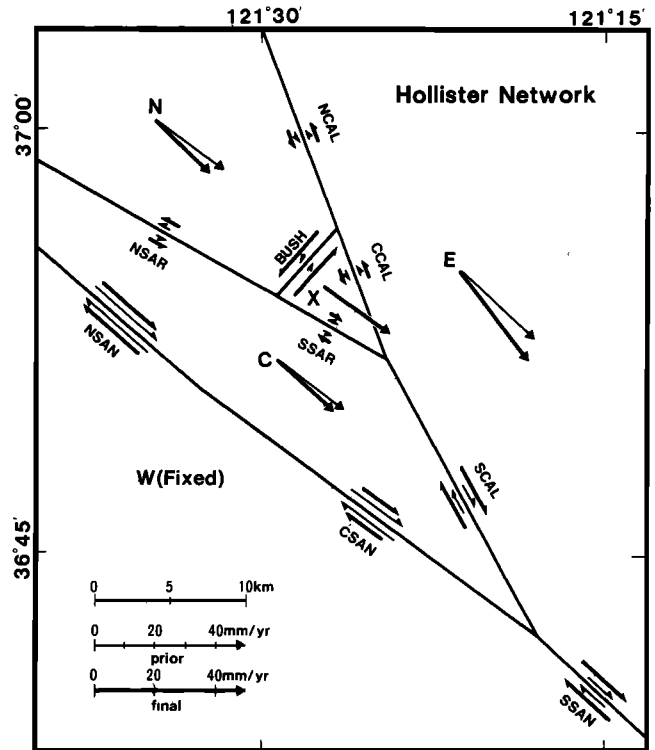


Fig. 5. Map showing block boundaries, with prior and final estimates of block velocities and dislocation rates. Thin arrows show prior estimates, thick arrows final estimates. Inner paired half arrows on each fault segment show prior estimates of fault slip rate, while outer half arrows show final estimates. Note that fault slip rate is the slip deficit (see Figure 1) and not the creep rate nor the relative block velocity. Final estimates are based on data set 83/92.

TABLE 1. Block Velocities (Data Set 83/92)

Block	Model	East, mm/yr	Res, %	North, mm/yr	Res, %	Magni- tude, mm/yr	Direc- tion, deg
W	prior	0 ± 0	...	0 ± 0	...	0	...
	final	0 ± 0	0	0 ± 0	0	0	...
E	prior	25 ± 5	...	-23 ± 5	...	34	S48E
	final	23 ± 2	93	-30 ± 2	94	38	S38E
C	prior	22 ± 5	...	-16 ± 5	...	28	S53E
	final	19 ± 3	92	-17 ± 2	94	26	S49E
N	prior	22 ± 5	...	-16 ± 5	...	28	S53E
	final	18 ± 3	91	-18 ± 3	92	26	S45E
X	prior	22 ± 5	...	-16 ± 5	...	28	S53E
	final	22 ± 10	0	-16 ± 10	0	28	S53E

"Res" is resolution, expressed as percentage of maximum possible.

where  $z$  is the depth from the earth's surface and  $\mu$  is the rigidity of the crust, assumed to be 40,000 MPa (400 kbar). The maximum offset occurs at  $z = 0$ ;

$$u_0 = 2aS/\mu \quad (44)$$

In terms of the maximum offset the stress drop is

$$S = \mu u_0/2a \quad (45)$$

on the displaced part of the fault.

If the true displacement obeyed (43), our estimate of the dislocation magnitude  $D$  would be close to  $u_0$  (the offset at the earth's surface) because the dislocation magnitude is well resolved if there are stations near the fault. We would estimate a fault width " $W$ " somewhat less than " $a$ ":

$$W = \pi a/4 \quad (46)$$

represents a "strain-averaged" depth such that the integral of displacement offset with respect to depth is the same for our model and for the Knopoff model. In terms of our model parameters the stress drop on the fault is

$$S = \pi\mu D/8W \quad (47)$$

Differentiating with respect to time, we have

$$\dot{S} = \pi\mu\dot{D}/8W \quad (48)$$

which gives the rate of stress accumulation on the fault in terms of the estimated quantities  $\dot{D}$  and  $W$ . We compute this quantity routinely, as well as its asymptotic variance

$$\text{Var}(\dot{S}) = (\pi\mu/8W)^2 [\text{Var}(\dot{D}) - 2(\dot{D}/W) \text{Cov}(\dot{D}, W) + (\dot{D}/W)^2 \text{Var}(W)] \quad (49)$$

The uncertainty reported below is the standard deviation or square root of the variance.

Assuming a periodic model for stress accumulation and release, we can calculate the recurrence interval of the largest earthquakes in terms of their stress drop and the stress accumulation rate. This recurrence time is  $t = S_0/|\dot{S}|$ , or in terms of the primary estimated parameters:

$$t = 8S_0W/\pi\mu|\dot{D}| \quad (50)$$

where  $S_0$  is the seismic stress drop. We calculate the recurrence time  $t$  assuming that  $S_0 = 10$  MPa (100 bars). Of course, there is plenty of doubt about the proper value for  $S_0$  and about the validity of the simple periodic earthquake model. Nevertheless, the reported recurrence time may be used to compare the relative behavior of different fault segments.

Pushing the model yet further, we can calculate the amount of slip  $D_s$  expected for periodic large earthquakes. It is simply the cumulative slip deficit between large events,  $D_s = \dot{D}t$ . Equivalently, it is the amount of slip required to produce a stress increment equal to the assumed stress drop. In terms of the estimated parameters we have

$$D_s = \text{sgn}(\dot{D})(8S_0W/\pi\mu) \quad (51)$$

A negative value of  $\dot{D}$ , and hence  $D_s$ , implies an eventual left-lateral earthquake.

#### 4.5. Prior Estimates

Table 1 shows prior estimates of the block parameters, along with final estimates to be discussed below. We base our prior estimates of the block parameters on the neotectonic studies of *Herd* [1979], summarized by *Ellsworth et al.* [1981]. We choose relative block velocities such that there is very little convergence (or divergence) at the block boundaries because there is no geologic evidence for significant motion normal to any of the faults. We fix the origin of coordinates

TABLE 2. Primary Fault Parameters (Data Set 83/92)

Fault	Model	$\dot{D}$ , mm/yr	Res, %	$W$ , km	Res, %	$\delta$ , deg	Res, %	$\lambda$ , deg	Res, %
NSAN	prior	27 ± 5	...	10 ± 5	...	85 ± 10	...	180 ± 10	...
	final	25 ± 4	73	9 ± 4	74	95 ± 12	57	177 ± 11	57
CSAN	prior	22 ± 5	...	5 ± 3	...	80 ± 10	...	180 ± 10	...
	final	16 ± 4	84	11 ± 4*	61	79 ± 9	79	154 ± 10*	72
SSAN	prior	9 ± 5	...	5 ± 3	...	85 ± 10	...	180 ± 10	...
	final	20 ± 8*	22	11 ± 5*	16	93 ± 19	3	175 ± 19	1
SCAL	prior	7 ± 5	...	10 ± 5	...	95 ± 10	...	180 ± 10	...
	final	20 ± 5*	74	0 ± 1	100	108 ± 11	66	201 ± 6*	91
CCAL	prior	-3 ± 5	...	5 ± 3	...	90 ± 10	...	180 ± 10	...
	final	-6 ± 3	89	6 ± 5	21	83 ± 17	19	191 ± 15	38
NCAL	prior	-3 ± 5	...	5 ± 3	...	90 ± 10	...	180 ± 10	...
	final	-7 ± 3	89	12 ± 5*	12	111 ± 17*	19	173 ± 17	19
NSAR	prior	-3 ± 5	...	10 ± 5	...	80 ± 10	...	180 ± 10	...
	final	-8 ± 2	93	15 ± 8	26	42 ± 14*	44	206 ± 17*	25
SSAR	prior	-3 ± 5	...	10 ± 5	...	80 ± 10	...	180 ± 10	...
	final	5 ± 7	42	2 ± 3	88	63 ± 19	8	181 ± 19	4
BUSH	prior	-3 ± 5	...	10 ± 10	...	90 ± 10	...	180 ± 10	...
	final	-21 ± 6*	67	3 ± 2	99	59 ± 15*	40	178 ± 12	58

"Res" is resolution, expressed as percentage of maximum possible.

\*Final estimates that differ from prior estimates by more than 2 prior standard deviations.

TABLE 3. Derived Parameters (Data Set 83/92)

Fault	Model	Block Slip, mm/yr	Block Convergence, mm/yr	Fault Slip, mm/yr	Fault Convergence, mm/yr	Creep Rate, mm/yr	Stress Rate, kPa/yr	Recurrence Time, years	Seismic Slip, m
NSAN	prior	27 ± 5	-3 ± 5	27 ± 5	0 ± 0	0 ± 7	43 ± 22	230 ± 123	6.4 ± 3.2
	final	26 ± 3	0 ± 1	25 ± 4	0 ± 1	0 ± 6	43 ± 19	230 ± 97	5.8 ± 2.6
CSAN	prior	28 ± 5	0 ± 5	22 ± 5	0 ± 1	6 ± 7	68 ± 43	143 ± 91	3.2 ± 1.9
	final	25 ± 3	2 ± 1	15 ± 4	1 ± 1	11 ± 5	25 ± 6	415 ± 120	6.8 ± 2.2
SSAN	prior	34 ± 5	0 ± 5	9 ± 5	0 ± 0	26 ± 7	28 ± 22	370 ± 308	3.2 ± 1.9
	final	37 ± 3	7 ± 1	20 ± 9	0 ± 1	17 ± 9	31 ± 22	334 ± 243	6.7 ± 3.4
SCAL	prior	7 ± 7	1 ± 7	7 ± 5	0 ± 0	0 ± 9	12 ± 9	895 ± 772	6.4 ± 3.2
	final	13 ± 2	3 ± 1	18 ± 4	2 ± 2	-5 ± 5	688 ± 1147	13 ± 23	0.3 ± 0.4
CCAL	prior	7 ± 7	-1 ± 7	-3 ± 5	0 ± 0	10 ± 9	-9 ± 15	1135 ± 2140	-3.2 ± 1.9
	final	13 ± 10	4 ± 10	-6 ± 3	0 ± 0	19 ± 11	-15 ± 15	623 ± 587	-4.0 ± 3.3
NCAL	prior	7 ± 7	-1 ± 7	-3 ± 5	0 ± 0	10 ± 9	-9 ± 15	1135 ± 2140	-3.2 ± 1.9
	final	13 ± 3	-1 ± 1	-7 ± 3	0 ± 1	20 ± 4	-9 ± 6	1047 ± 629	-7.7 ± 3.5
NSAR	prior	0 ± 7	0 ± 7	-3 ± 5	0 ± 0	3 ± 9	-6 ± 9	2121 ± 3690	-6.4 ± 3.2
	final	0 ± 2	2 ± 2	-7 ± 2	3 ± 2	7 ± 4	-6 ± 6	1297 ± 801	-9.8 ± 5.3
SSAR	prior	0 ± 7	0 ± 7	-3 ± 5	0 ± 0	3 ± 9	-6 ± 9	2121 ± 3690	-6.4 ± 3.2
	final	2 ± 10	-2 ± 10	5 ± 7	0 ± 1	-3 ± 13	52 ± 185	191 ± 687	1.0 ± 2.1
BUSH	prior	0 ± 7	0 ± 7	-3 ± 5	0 ± 0	3 ± 9	-6 ± 9	2121 ± 4125	-6.4 ± 6.4
	final	4 ± 10	1 ± 10	-21 ± 6	0 ± 2	25 ± 11	-117 ± 93	84 ± 68	-1.8 ± 1.0

on the western block W by setting its velocity to  $0.0 \pm 0.01$  mm/yr. The prior estimates for block E imply a motion of 34 mm/yr in the direction S48°E. We choose a prior uncertainty of 5 mm/yr in both the east and north directions, so that most published estimates for this region fall within two standard deviations of our prior estimates. According to our prior estimates, blocks N, C, and X all move at the same rate; this value is fixed at 28 mm/yr in the direction S53°E with respect to block W by the requirement that the absolute convergence be small.

According to the global plate model of *Minster and Jordan* [1978] the relative motion of the North American plate with respect to the Pacific plate in central California would be about 56 mm/yr in the direction S35°E. Their model is based on rates of seafloor spreading, transform fault azimuths, and earthquake slip vectors. The relative plate velocity provides an upper limit to block motion in the Hollister area. *Hall* [1981] showed that average right-lateral motion on the San Simeon-Hosgri fault zone probably equalled 10–15 mm/yr during the last 3 m.y. Presumably, comparable rates of motion have occurred on the San Gregorio fault system or on other offshore faults west of the Hollister network. Some displacement may also occur east of the network, but the low seismicity there suggests very limited displacement.

Table 2 shows prior estimates of the fault parameters, along with final estimates to be discussed below. We estimate the dislocation rates to be the difference between the relative block motion and the observed creep rate. Average creep rates have been reported by *Burford and Harsh* [1980], *Ellsworth et al.* [1981], and *Schulz et al.* [1982]. We assume compromise creep values as follows: 0 mm/yr for NSAN, 6 mm/yr for CSAN, 26 mm/yr for SSAN, 0 mm/yr for SCAL, 10 mm/yr for CCAL and NCAL, 3 mm/yr for NSAR and SSAR, and 0 mm/yr for BUSH. For data set 83/92 we supply one additional prior datum that is not shown in Table 2. We set the creep rate on the northern San Andreas fault equal to  $0 \pm 1.0$  mm/yr. Without this prior datum the best fitting model would have a physically unreasonable negative creep rate. The other parameters (dip angle  $\delta$ , slip angle  $\lambda$ , and fault width  $W$ ) are estimated from focal mechanisms of regional earthquakes [*Bolt et al.*, 1968] and distributions of microearthquakes in this area [*Eaton et al.*, 1970]. These studies show that

throughout the region the fault dip is nearly vertical, and most events have right-lateral strike-slip focal mechanisms. The strike directions agree with the orientation of the major fault traces. Since the lower bound of brittle seismicity is about 15 km in the Hollister area, the depth of the locked part may be less than 15 km.

Prior values of the derived parameters are shown in Table 3. The block slip rate and the block convergence rate depend only on the relative block velocities. For the prior model the block slip rate is greatest on the San Andreas fault, quite modest on all segments of the Calaveras, and near zero everywhere else. The fault slip rates are equal to the dislocation rates in the prior model because the slip angle was assumed to be 180° (right-lateral strike slip) for all faults. Some of the fault slip rates are negative, implying a left-lateral slip deficit, because the observed creep rate exceeds the block slip rate for these faults.

## 5. RESULTS

### 5.1. Quality of Fit

Table 4 summarizes the level of agreement between the model and the data for each data set. Both the prior model and the appropriate final model are compared against each data set. The top two lines give the trace of the resolution matrix and the percentage of information provided by the trilateration observations. Resolution for the prior model is zero by definition. The resolution is best for data set 83/92. However, no data set provides as much as 50% resolution. Clearly, many features of each final model depend strongly on the prior estimates. Specific resolution estimates for each parameter will be discussed below. The next three rows of Table 4 describe the fit of the models to the prior data; rows 6–8 describe the fit to the trilateration data; and the last three rows describe the fit to the combined trilateration and prior data. Within each group, the top row gives the dimensionless sum of squared residuals, standardized by the appropriate covariance matrix. The next row gives the number of degrees of freedom “ $df$ ” in the data after fitting. The expected value of the sum of squared residuals is just the  $df$ . The quantity “rms” is the square root of the ratio of the two quantities above. It is probably the best index of quality of fit, being about 1.0 if the

TABLE 4. Quality of Fit

	Data Set					
	78/69		78/85		83/92	
	Prior Model	Final Model	Prior Model	Final Model	Prior Model	Final Model
$r$	0	18	0	21	0	24
Res, %	0	39	0	45	0	48
$d'D^{-1}d$	0	68	0	66	0	113
$df$ (prior)	0	18	0	21	0	25
rms (prior)	...	1.9	...	1.8	...	2.1
$e'E^{-1}e$	1049	82	1459	133	3218	234
$df$ (obs)	69	51	85	64	92	68
rms (obs)	3.9	1.3	4.1	1.4	5.9	1.9
$s$	1049	150	1459	199	3218	347
$df$ (all)	69	69	85	85	93	93
rms (all)	3.9	1.5	4.1	1.5	5.9	1.9

The  $r$  is the trace of resolution matrix; Res =  $100r/m$ , where  $m$  is the number of adjustable parameters (46);  $d'D^{-1}d$ ,  $e'E^{-1}e$ , and  $s$  are defined as in equations (24)–(26);  $df$  (prior) =  $p + r - m$ , where  $p$  is the number of prior data;  $df$  (obs) =  $n - r$ , where  $n$  is the number of observed data;  $df$  (all) =  $n + p - m$ .

model fits the data as expected, less than 1.0 for a better fit, and so on.

It is apparent from Table 4 that the rms residual is greater than one for all cases. Thus the uncertainties in the data have been underestimated by a factor of about 2, or the model is not completely correct. Of course, every model is deficient in some way, and ours neglects several effects including those listed in section 3.3. The prior model does not fit any of the trilateration data sets very well. For each data set the final model reduces the sum of squared residuals by an order of magnitude compared to the prior model. Comparing results for data sets 78/69 and 78/85, we see that the additional trilateration data in the latter one can be fitted reasonably well without violating the prior observations; rms (obs) and rms (prior) are about the same for both data sets. The additional trilateration data in data set 83/92 are harder to fit; the rms residuals to both the prior and observed data increase substantially compared to data sets 78/69 and 78/85.

### 5.2. Summary of Results for All Data Sets

Figure 6 gives a simple representation of the right-lateral slip rate versus depth for each fault according to each of the data sets. The rate shown for shallow depth is the creep rate, and for greater depth it is the block slip rate, with the transition occurring at a depth nearly equal to the fault width. A negative creep rate implies left-lateral creep. If the creep rate exceeds the block slip rate, the implication is that right-lateral shear stress has been reduced during the observation period or, equivalently, that left-lateral shear stress has increased.

The most important inference to be drawn from Figure 6 is that the block slip rate varies greatly from fault to fault, but this rate does not depend much on which data set is used. For every data set the block slip rate is greatest on the fault SSAN, followed by NSAN and CSAN in that order. The final estimates of block slip rates are generally close to the prior estimates, except for the three segments of the Calaveras fault, where the prior estimate was too low, and for the poorly resolved Busch fault.

Estimates for the creep rate are not as stable as those for the block slip rate. We see large variability in creep rate for the faults SSAN, NCAL, and SSAR. The estimated fault width is also variable, especially on NSAN and SSAN. However, the

southern Calaveras fault, SCAL, is always very shallow (effectively zero for data set 78/69).

Figure 6 reveals a few embarrassing features that we do not believe geophysically reasonable. One is the negative creep rate estimated for the SCAL fault by all data sets that include the lines to stations HLS and PRR. However, this feature is poorly resolved and not statistically significant; we interpret this value to mean "effectively zero." Another quirk is the apparent right-lateral block motion and creep along the BUSH fault, which suffered a left-lateral earthquake in 1974 [Savage *et al.*, 1976]. Neither the block slip rate nor the creep rate is well resolved or statistically significant. What is clear about the BUSH fault is that it plays only a bit part in the drama of central California tectonics. The same is true of NSAR and SSAR; their primary influence is to increase the uncertainty of the other estimates. Fortunately, we can include them easily enough in our models, and the damage that they cause is limited by the prior estimates of their activity. By including them in the model we can demonstrate, rather than just assume, their lack of geodetic influence.

### 5.3. Detailed Results for Data Set 83/92

Final estimates for the most complete data set, 83/92, are summarized graphically in Figure 5. Please note that the paired arrows on each fault in Figure 5 represent the dislocation rate (that is, the slip deficit), not the block slip rate nor the creep rate. Numerical values for the block velocities are given in Table 1, while Tables 2 and 3 list the estimates for the primary and derived fault parameters, respectively.

An important conclusion from Figure 5 is that the final estimates of block velocity agree extremely well with the prior estimates. The only significant change is for block E; here the vector difference between the final and prior velocities has a magnitude of about 7 mm/yr. The resolution of the velocity estimates is very high (over 90%; see Table 1) for all blocks except W and X. Block W is not resolved simply because it is fixed as the reference block, and block X has no monuments on it. The high resolution for blocks E, C, and N means that their velocities are determined almost entirely by the trilateration data, with little sensitivity to the prior estimates. Because the prior data are based on geological data, our result implies that the geodetic data are not only consistent with geologic data but also lead independently to the same answer. Remarkably, the average block motion over the last decade is close to the average rate for many thousands of years, within the estimation errors of a few millimeters per year. This suggests that the block motion is driven by some relentless engine that cares little about earthquakes or other episodic annoyances at the earth's surface.

The final model has the E block moving at 38 mm/yr in the direction S38°E with respect to the W block. The final velocity vectors all point a bit more southward than the prior estimates, implying a small amount of block convergence.

The estimated dislocation rates (or slip deficits) do not agree well with the prior estimates. The largest slip deficit occurs on fault NSAN, while SSAN, SCAL, and BUSH also have substantial dislocation rates. The final values for these faults are more than double the prior estimates.

Table 2 gives more detailed results for the fault parameters estimated from data set 83/92. An important conclusion is that the fault width varies considerably from place to place, ranging from less than 1 km on SCAL to 15 km on NSAR. The fault width affects the computed line length rates in a highly nonlinear way, especially for fault width less than 5 km, so the final uncertainty and resolution estimates should not be taken

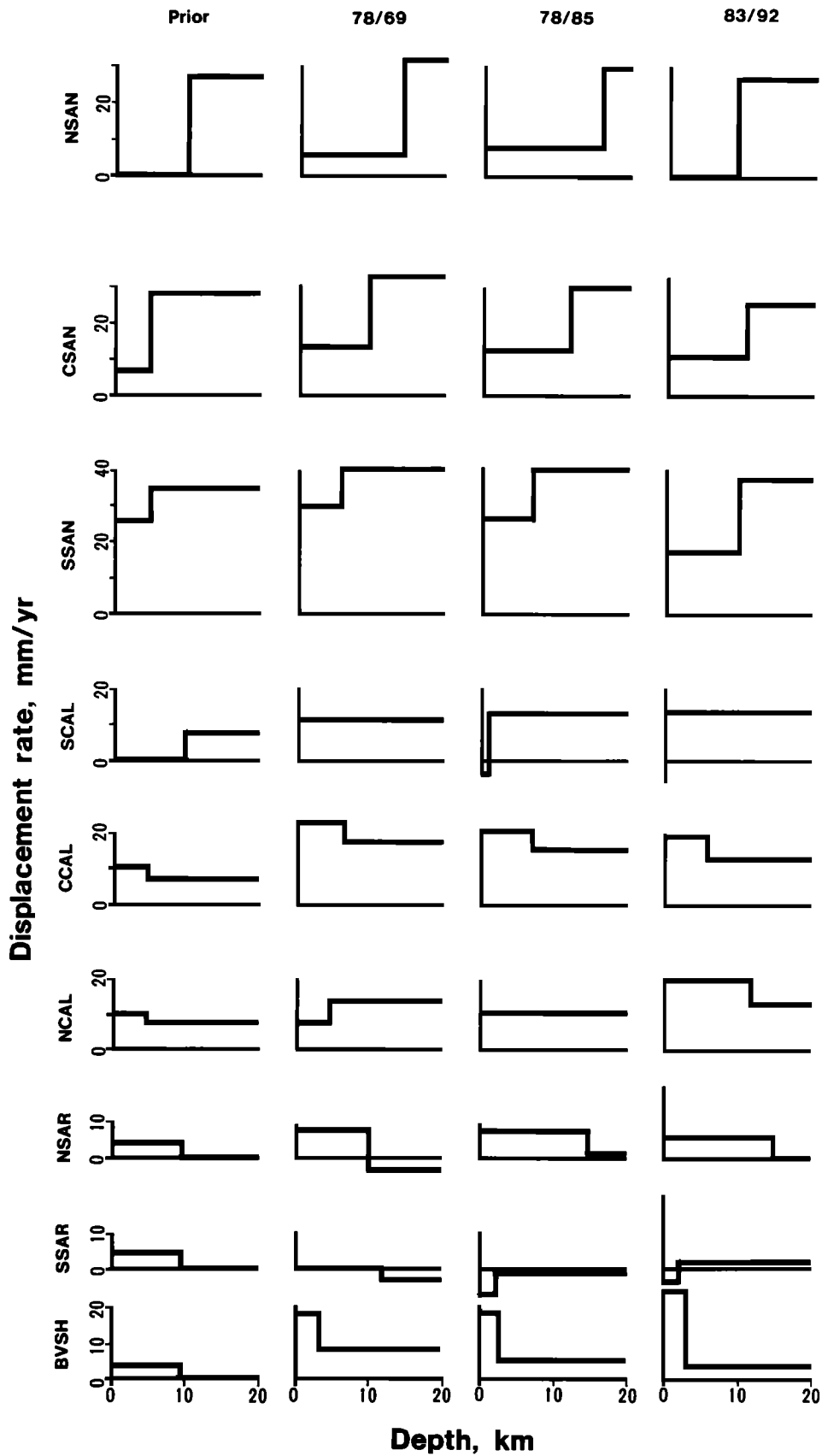


Fig. 6. Estimated displacement rate versus depth on each of nine fault segments for the prior model and for final models based on three different data sets. "Depth" is measured downdip in the fault plane, so that the transition from shallow to deep slip rate occurs at depth  $W$ . The displacement rate at zero depth is the creep rate; displacement rate at 20 km depth is the relative block velocity; and the difference is the horizontal component of the dislocation rate.

too seriously in these cases. Nevertheless, SCAL, SSAR, and BUSH must be very shallow. Fault width resolution exceeds 50% for five faults: NSAN, CSAN, SCAL, SSAR, and BUSH. The last four achieve this distinction because they are blessed with stations both near to and far from the fault trace, so that shallow and deep slip can be distinguished. Resolution of fault width on NSAN is at first surprising because it is not so blessed. However, the theoretical displacement pattern for a rectangular fault includes relatively large displacements near the corners, and the pattern of these displacements responds strongly to the fault depth. Thus monuments HWY, HLT, MRS, and SRG are all sensitive to the fault width of NSAN.

As explained in section 3.3, the standard deviations of the final estimates may be greater than the prior uncertainties. This occurs because we reestimate the uncertainties of all data based on the sum of squared residuals, which is greater than expected. The minimum value of  $s$  in (24) for this data set is 347, while its expected value is 93. The final uncertainties are thus larger by a factor of  $(347/93)^{1/2} = 1.9$  than they would be if we used only the prior uncertainties for the data and initial estimates.

Final estimates that differ from the prior estimates by more than two prior standard deviations we call "surprises," and we label them with asterisks in Table 2. There are 12 such surprises out of 36 fault parameters, clearly indicating that we have underestimated the errors in the prior model. As shown in section 5.1, we also underestimated observational errors by about the same factor. Some of the most significant surprises are for SSAN, where the dislocation rate and fault width both doubled, and for NCAL, where the dip angle changed considerably and the fault width doubled.

The stress related parameters  $\dot{S}$ ,  $t$ , and  $D$ , (Table 3) are controlled largely by the fault width  $W$  and the dislocation rate  $\dot{D}$ . The stress accumulation rate  $\dot{S}$  is highest for those faults with a large dislocation rate and small fault width. Fault SCAL has by far the highest stress accumulation rate by virtue of its small width. However, its uncertainty is also very large. Only the northern and central San Andreas have estimated stress accumulation rates exceeding two standard deviations. The recurrence time is inversely proportional to the stress accumulation rate; it is greatest for NSAR, NCAL, and CCAL. Clearly the amounts of seismic slip must be taken with a grain of salt, since we assumed a 10-MPa stress drop on the entire fault patch, and its uncertainty is quite large. However, the large seismic slip estimates should remind us that any fault locked to a depth of 10 km or so may be capable of rather large earthquakes after a few hundred years of stress accumulation. Fault SCAL is clearly different from the others; because of its relatively high dislocation rate and small fault width, it should have frequent but never very large events.

A measure of the long-term seismic risk of a fault segment is the accumulation rate of "aseismic moment," which is proportional to the product of the slip deficit, the fault width, and the length of the fault segment. By this criterion the most dangerous fault is the northern San Andreas, followed by the southern and central San Andreas. Note that in spite of its large creep rate, the southern San Andreas still has a large slip deficit. The northern Calaveras and the northern Sargent faults have moderately high accumulation rates of aseismic moment with negative sign, which means that the right-lateral shear stress is decreasing. A slightly unrealistic prior estimate may cause the negative stress rate on NCAL and NSAR, although the 1979 Coyote Lake earthquake could have released more stress than has accumulated on NCAL.

#### 5.4. Correlated Estimation Errors

The correlation between estimates of any pair of parameters may be determined by their correlation coefficient,

$$\rho_{ij} = C_{ij}/(C_{ii}C_{jj})^{1/2}$$

where  $C_{ij}$  are the elements of the asymptotic covariance matrix  $C'$  of equation (34). The correlation coefficient must lie between  $-1.0$  and  $1.0$ . Overestimation of one parameter implies probable overestimation of the other if two parameters are positively correlated. This situation arises when the data are especially sensitive to the difference between the two parameters. Similarly, if two parameters are negatively correlated, a positive estimation error for one suggests a negative error for the other and that the data are sensitive to their sum. Note that a large correlation coefficient does not mean that the two variables are more uncertain than they would be if uncorrelated. When the prior covariance matrix is diagonal as it is here, large correlation coefficients generally occur for the well-resolved parameters.

The largest correlations involve the eastward velocity of block C. This parameter has a positive correlation with the dislocation rate on CSAN (0.96) and with the eastward velocity of blocks E and N (0.94 and 0.79, respectively); it has a negative correlation ( $-0.87$ ) with the northward component of block C. Similarly, the eastward velocity of block E is correlated positively with the dislocation rate on CSAN (0.90) and the eastward velocity of block N (0.81) but negatively with the northward velocity of block C ( $-0.78$ ). The dislocation rate on SSAR is negatively correlated with fault width on the same fault ( $-0.93$ ). Thus if we underestimated the fault width, we may have overestimated the dislocation rate. However, our estimated dislocation rate for SSAR is already quite small. On the BUSH fault the correlation between dislocation rate and fault width is 0.81, opposite in sign to that for SSAR. The negative dislocation rate on BUSH might be caused by our underestimating the fault width. However, the fault width is well resolved, indicating that a small fault width fits the data much better than a large one. The northward velocity for block C and the dislocation rate on CSAN share a negative correlation ( $-0.86$ ). All of the other correlation coefficients lie between  $-0.70$  and  $0.70$ , and none reveals any particularly fascinating secrets about the parameter estimates.

## 6. DISCUSSION

Virtually all displacements seen in the trilateration data are aseismic. Only two significant earthquakes occurred during the period of this study, on November 28, 1974, and August 6, 1979. The 1974 event, known as the "Thanksgiving Day earthquake," occurred on fault segment BUSH. It had a magnitude 5.2 and caused 150 mm of left-lateral slip on a rectangular patch 3 km long and 5 km wide (extending from 5 to 10 km depth) according to the dislocation model of *Savage et al.* [1976]. This event might be expected to cause left-lateral surface displacement on BUSH or apparent right-lateral creep on SSAR or CCAL during the period from 1971 to 1983. However, the estimated creep rate on BUSH is right lateral for all data sets, and there is no significant difference between the estimates from the earlier and later data. We do not believe that the 1974 event had any substantial effect on the estimated BUSH creep rate, which is not significantly different from zero anyway. This earthquake may have caused apparent right-lateral creep on CCAL, however. The 1979 Coyote Lake earthquake was a magnitude 5.7 event on the northern Calaveras fault, outside of the Hollister network. According to

Bouchon [1982] this event caused 150–200 mm of right-lateral slip on a 14-km-long fault segment extending from about 1 km to about 10 km depth. The effect of this event should be to increase the apparent right-lateral creep rate in the more recent data sets for the fault NCAL. In fact, a modest increase of about 5 mm/yr does occur in the average creep rate for data set 83/92 compared with the others. The right-lateral creep on NCAL is significantly different from zero, but the change between the earlier and later data is not. The theoretical surface displacement from the Coyote Lake event would be measurable only at station CND, whose displacement is not well determined because there are no stations north of it. Block slip on NCAL does exceed its prior estimate by 6 mm/yr (Table 3), and seismic and postseismic effects of the Coyote Lake event may contribute to this excess. However, their contributions are unlikely to exceed the estimated uncertainty of 3 mm/yr. Thus neither the 1974 nor the 1979 event had any significant impact on the average slip rates for the period from 1971 to 1983.

The relative block motion and the aseismic slip rate along the fault system in the Hollister area have also been estimated by Savage *et al.* [1979] and by Thatcher [1979]. Savage *et al.* used the same data set that we call 78/85. Thatcher used 233 triangulation data, 16 trilateration data, and one astronomic datum. His triangulation data cover the interval from 1885 to 1976. Both Savage *et al.* and Thatcher approximated the fault system by vertical strike-slip fault segments and divided each segment into shallow and deep slip zones. The shallow slip rates (creep rates) and deep slip rates (block slip rates) obtained by the former investigators are summarized in Table 5, along with our estimates for data set 83/92. We agree moderately well with Savage *et al.* but not so well with Thatcher. On the northern and central San Andreas we agree with Savage *et al.* on a block slip rate of about 25 mm/yr. Thatcher infers a much greater block slip rate, partly because he constrains the fault width to 15 km and partly because he used one block slip value to represent the combined effects of the San Andreas and Calaveras. Thatcher tried other values of fault width, but he found that 15 km provided the best fit to the data. He used triangulation data spanning a much wider zone (60 km) than the trilateration data we used. His data set might be more sensitive to the fault width than ours. However, he did not report an uncertainty or resolution estimate for fault width. On the southern San Andreas we obtain a much smaller creep rate than either Savage *et al.* or Thatcher, but the differences are less than two standard deviations. The differences may be caused by differences in the assumed range of the southern San Andreas fault. Thatcher included data from farther south, where the observed creep rate is larger. Savage *et al.* assumed a shallow slip rate rather than estimating it from the geodetic data. Our estimate should be appropriate only for latitudes north of 36°40', where the trilateration monuments lie. On the southern Calaveras fault we obtain a shallower fault depth than the others; Savage *et al.*'s value of 5 km is consistent with ours, but Thatcher's assumed value of 15 km does not agree with the recent trilateration data. For the central and northern Calaveras, all three estimates show the creep rate exceeding the block slip, implying a decrease in right-lateral stress (or an increase in left-lateral stress). When we used the earlier data sets (78/69 and 78/85 in Figure 6), the NCAL creep rate was less than or equal to the block slip rate. Thus the apparent stress reduction on NCAL may result from the 1979 earthquake. The lack of block slip on the Calaveras in Thatcher's model should not cause alarm, as he assigned all of the rela-

TABLE 5. Comparison With Published Solutions

Fault	This Work (83/92)	Savage <i>et al.</i> [1979]	Notes	Thatcher [1979]	Notes
<i>Fault Width, km</i>					
NSAN	9 ± 4	5.0	t	15.0	f
CSAN	11 ± 4	5.0	t	15.0	f
SSAN	11 ± 5	15.0	f	15.0	f
SCAL	0 ± 1	5.0	f	15.0	f
CCAL	6 ± 5	5.0	f	15.0	f
NCAL	12 ± 5	5.0	f	15.0	f
NSAR	15 ± 8	5.0	t	0.0	f
SSAR	2 ± 3	5.0	t	0.0	f
BUSH	3 ± 2	0.0	f	0.0	f
<i>Creep Rate, mm/yr</i>					
NSAN	0 ± 0	0.0	f	0.0	f
CSAN	11 ± 5	8.9 ± 1.5		15.5 ± 3.0	a
SSAN	17 ± 9	32.0	f	29.7 ± 1.8	a
SCAL	-5 ± 5	0.0	f	13.0 ± 2.0	
CCAL	19 ± 10	14.9 ± 1.8		13.0 ± 1.6	a
NCAL	20 ± 4	14.9 ± 1.8		13.0 ± 1.6	a
NSAR	6 ± 4	3.9 ± 1.4		0.0	f
SSAR	-3 ± 13	3.9 ± 1.4		0.0	f
BUSH	25 ± 11	0.0	f	0.0	f
<i>Block Slip Rate, mm/yr</i>					
NSAN	26 ± 3	22.2 ± 3.1		38.0 ± 3.0	
CSAN	25 ± 3	22.2 ± 3.1		38.0 ± 3.0	
SSAN	37 ± 2	38.0	f	38.0 ± 3.0	
SCAL	13 ± 2	14.4 ± 2.2		0.0	f
CCAL	13 ± 10	14.4 ± 2.2		0.0	f
NCAL	13 ± 3	14.4 ± 2.2		0.0	f
NSAR	0 ± 2	0.0	f	0.0	f
SSAR	2 ± 10	0.0	f	0.0	f
BUSH	4 ± 10	0.0	f	0.0	f

Notes: a, average of values for several fault segments; f, fixed; t, determined by trial and error.

tive block motion to the San Andreas fault, which he considered to be the plate boundary. Our value of 38 mm/yr relative velocity between blocks E and W is quite consistent with Thatcher's 38 mm/yr for the San Andreas–Calaveras system. Our results show that the Calaveras is also part of the plate boundary, and other faults outside the trilateration network are presumably part of the plate boundary as well. New features of our work not present in the others are (1) the variation of fault width from place to place, even on a given fault, (2) the ability to distinguish block motion from near-surface fault motion and to compare block motion with geological estimates, and (3) a method to test the importance of minor faults such as NSAR, SSAR, and BUSH, which could have been significant, although they have proved to be unimportant.

Our results clearly show that aseismic deformation is very important in plate tectonics. While some of the near-surface slip on the northern Calaveras fault may result from the 1979 earthquake, all of the block motion and most of the near-surface motion has been aseismic. Every fault segment except NSAR, SSAR, and BUSH is subject to aseismic deformation below some depth, which varies with fault segment. Any attempt to match the rate of seismic moment release to the value required by plate tectonics must include the effects of this aseismic motion and the varying thickness of the brittle zone on each fault.

By using the Bayesian inversion procedure outlined here, we are able to include arbitrarily many fault segments, without

regard to the adequacy of the data to resolve all the parameters. Unresolved parameters cause some increase in the uncertainty of the other parameters, as they should, but they do not cause any problems in the inversion procedure. With this method it is theoretically possible to make a very detailed map of stress accumulation in a region with many interacting faults. The usefulness of such a map depends of course on the quantity and quality of the geodetic data that go into it.

The agreement between the observations and the predictions of our model does not prove that the model represents well the stress accumulation mechanism at plate boundaries. It may be possible to fit the data equally well with a model involving no faults or blocks at all. For example, viscous flow in the asthenosphere might cause tractions at the base of a lithosphere with variable thickness, causing a concentration of strain rate where the lithosphere is thin. Or the crust itself may be viscoelastic, with spatially varying rigidity and viscosity. One can generalize from our results to infer the properties of alternate models. The regions that we call blocks are characterized by the absence of significant internal deformation, so they must be regions of relatively thick crust or large viscosity. The "faults" are zones of strain concentration, and what we model as fault width is essentially the width of such a zone. The relative block velocity would correspond to the difference in flow rate across the array, and this is very well determined. The variation of some near-surface properties in any alternate model must be only weakly resolved, as are the fault parameters on some segments in our model.

The agreement of the inferred block velocities with geologically estimated fault slip rates, coupled with the good resolution of these parameters, strongly implies a steady pattern of flow in the asthenosphere. A further suggestion, somewhat more tenuous because resolution is lacking, is that the shallower slip rates vary more in time. This notion is clearly consistent with the fact that earthquakes, which produce episodic displacements, are limited to the upper crust in central California. Creep in the upper hundred meters or so is also variable and probably related in some way to earthquakes. An important feature just beyond our resolving ability is the temporal variability of aseismic slip motion at a few kilometers depth. We believe it likely that earthquakes are preceded by accelerated slip just at the boundaries, especially the lower boundaries, of the locked fault surfaces. With a greater density of monuments and with more frequent measurements it should be possible not only to detect but also to interpret the aseismic slip motions that trigger seismic catastrophes.

*Acknowledgments.* We gratefully acknowledge support from NASA via contract NAS5-26895 and grant NAG5-447 and from USGS via contract 14-08-0001-21243.

#### REFERENCES

- Bolt, B. A., C. Lomnitz, and T. V. McEvelly, Seismological evidence on the tectonics of central and northern California and Mendocino escarpment, *Bull. Seismol. Soc. Am.*, *58*, 1725-1767, 1968.
- Bouchon, M., The rupture mechanism of the Coyote Lake earthquake of 6 August 1979 inferred from near-field data, *Bull. Seismol. Soc. Am.*, *72*, 745-757, 1982.
- Burford, R. O., and P. W. Harsh, Slip on the San Andreas fault in central California from alignment array surveys, *Bull. Seismol. Soc. Am.*, *70*, 1233-1261, 1980.
- Eaton, J. P., W. H. K. Lee, and L. C. Pakiser, Use of microearthquakes in the study of the mechanics of earthquake generation along the San Andreas fault in central California, *Tectonophysics*, *9*, 259-282, 1970.
- Ellsworth, W. L., A. G. Lindh, W. H. Prescott, and D. G. Herd, The 1906 San Francisco earthquake and the seismic cycle, in *Earthquake Prediction: An International Review, Maurice Ewing Ser.*, vol. 4, edited by D. W. Simpson and P. G. Richards, pp. 126-140, AGU, Washington, D. C., 1981.
- Hall, C. A., Jr., San Luis Obispo transform fault and middle Miocene rotation of the western Transverse Ranges, California, *J. Geophys. Res.*, *86*, 1015-1031, 1981.
- Herd, D. G., Neotectonic framework of central coastal California and its implications to microzonation of the San Francisco Bay region, Progress on Seismic Zonation in the San Francisco Bay Region, edited by E. E. Brabb, *U.S. Geol. Surv. Circ.*, *807*, 3-12, 1979.
- Jackson, D. D., Interpretation of inaccurate, insufficient and inconsistent data, *Geophys. J. R. Astron. Soc.*, *28*, 97-109, 1972.
- Jackson, D. D., The use of a priori data to reduce non-uniqueness in linear inversion, *Geophys. J. R. Astron. Soc.*, *57*, 137-147, 1979.
- Jackson, D. D., and M. Matsu'ura, A Bayesian approach to nonlinear inversion, *J. Geophys. Res.*, *90*, 581-591, 1985.
- Knopoff, L., Energy release in earthquakes, *Geophys. J. R. Astron. Soc.*, *1*, 44-52, 1958.
- Matsu'ura, M., Inversion of geodetic data, I, Mathematical formulation, *J. Phys. Earth*, *25*, 69-90, 1977.
- Matsu'ura, M., and N. Hirata, Generalized least-squares solutions to quasi-linear inverse problems with a priori information, *J. Phys. Earth*, *30*, 451-468, 1982.
- Minster, J. B., and T. H. Jordan, Present-day plate motions, *J. Geophys. Res.*, *83*, 5331-5354, 1978.
- Okada, Y., Surface deformation due to shear and tensile faults in a half-space, *Bull. Seismol. Soc. Am.*, *75*, 1135-1154, 1985.
- Savage, J. C., M. A. Spieth, and W. H. Prescott, Preseismic and coseismic deformation associated with the Hollister, California, earthquake of November 28, 1974, *J. Geophys. Res.*, *81*, 3567-3574, 1976.
- Savage, J. C., W. H. Prescott, M. Lisowski, and N. E. King, Geodolite measurements of deformation near Hollister, California, 1971-1978, *J. Geophys. Res.*, *84*, 7599-7615, 1979.
- Savage, J. C., W. H. Prescott, M. Lisowski, and N. E. King, Strain accumulation in southern California, 1973-1980, *J. Geophys. Res.*, *86*, 6991-7001, 1981.
- Schulz, S. S., G. M. Mavko, R. O. Burford, and W. D. Stuart, Long-term fault creep observations in central California, *J. Geophys. Res.*, *87*, 6977-6982, 1982.
- Tarantola, A., and B. Valette, Generalized nonlinear inverse problems solved using the least squares criterion, *Rev. Geophys.*, *20*, 219-232, 1982.
- Thatcher, W., Systematic inversion of geodetic data in central California, *J. Geophys. Res.*, *84*, 2283-2295, 1979.
- Weertman, J., Relationship between displacements on a free surface and the stress on a fault, *Bull. Seismol. Soc. Am.*, *55*, 945-953, 1965.
- M. Matsu'ura, Geophysical Institute, Faculty of Science, University of Tokyo, Bunkyo-ku, Tokyo 113, Japan.
- A. Cheng, and D. D. Jackson, Department of Earth and Space Sciences, University of California, Los Angeles, CA 90024.

(Received January 24, 1986;  
revised May 22, 1986;  
accepted June 26, 1986.)